Hydrogenation of the $Ce(Rh_{1-x}Ir_x)Ga$ System: Occurrence of Antiferromagnetic Ordering in the Hydrides $Ce(Rh_{1-x}Ir_x)GaH_{1.8}$

B. Chevalier,*,† B. Heying,‡ U. Ch. Rodewald,‡ C. Peter Sebastian,‡ E. Bauer,§ and R. Pöttgen*,‡

Institut de Chimie de la Matière Condensée de Bordeaux (ICMCB), CNRS [UPR 9048], Université Bordeaux 1, 87 avenue du Docteur Albert Schweitzer, 33608 Pessac Cedex, France, Institut für Anorganische und Analytische Chemie, Universität Münster, Corrensstrasse 30, D-48149 Münster, Germany, and Institut für Festkörperphysik, Technische Universität Wien, Wiedner Hauptstrasse 8-10, A-1040 Wien, Austria

Received February 27, 2007. Revised Manuscript Received April 4, 2007

The ternary gallides $Ce(Rh_{1-x}Ir_x)Ga$ with $x = 0$, 0.54, and 1 were synthesized from the elements by arc-melting. The structures of these intermediate valence compounds were investigated on the basis of powder and single-crystal X-ray diffractometer data: TiNiSi type, *Pnma*, $a = 688.2(2)$, $b = 439.6(1)$, and $c = 788.9(1)$ pm, w$R2 = 0.0493$, 563 F^2 values, and 20 variable parameters for CeRhGa; $a = 685.5(1)$, $b = 436.0(1)$, and $c = 782.7(1)$ pm, w$R2 = 0.0685$, 563 F^2 values, and 21 variable parameters for $Ce(Rh_{0.46}Ir_{0.54})Ga$; and $a = 690.1(1)$, $b = 436.6(1)$ and $c = 785.2(2)$ pm, w$R2 = 0.0810$, 562 F^2 values, and 20 variable parameters for CeIrGa. The rhodium (or iridium) and gallium atoms build up three-dimensional [RhGa] and [IrGa] networks with Rh−Ga (or Ir−Ga) distances ranging from 265 to 267 pm (or from 265 to 269 pm). The cerium atoms fill distorted hexagonal channels within these networks with one short Ce−Rh (or Ce−Ir) contact (281 pm in CeRhGa, 283 pm in $Ce(Rh_{0.46}Ir_{0.54})Ga$, and 287 pm in CeIrGa). Hydrogenation leads to the formation of the hydrides $Ce(Rh_{1-x}Ir_x)GaH_{1.8}$ in going with a switch in structure type: ZrBeSi type, $P6_3/mmc$, $a = 437.3(1)$ and $c = 839.2(1)$ pm for $CeRhGaH_{1.8}$, $a = 440.1(1)$ and $c = 829.1(1)$ pm for $Ce(Rh_{0.46}Ir_{0.54})GaH_{1.8}$, and $a = 441.8(1)$ and $c = 823.3(1)$ pm for $CeIrGaH_{1.8}$. Susceptibility and specific heat measurements on the hydrides reveal stable trivalent cerium and antiferromagnetic ordering at low temperatures; the Néel temperature decreases with the rhodium content. Fitting of the susceptibility data of the hydrides considering the crystal field splitting and molecular field effects clearly revealed the doublet $\Gamma_9 = |\pm 3/2\rangle$ as the ground state. Electrical resistivity data and thermoelectric power measurements show the characteristics of Kondo systems.

Introduction

The cerium compounds CeTX (T = transition metal and X = element of the third, fourth, or fifth main group) are an outstanding class of intermetallics since they exhibit unusual physical properties like magnetic ordering with anomalously high-ordering temperatures, valence fluctuations, heavy-fermion behavior, Kondo semimetals or semiconductors, non-Fermi liquid behavior, or quantum phase transitions.[1−3] The different electronic and magnetic ground states arise from the hybridization between the 4f(Ce) orbitals and the conduction electrons.

The physical properties of these materials can be influenced through changes of the valence electron concentration either through substitution of the T or X component or via solid solutions $Ce(T_{1-x}T_x')X$ and $CeT(X_{1-y}X_y')$. Prominent recent examples are the systems $Ce(Rh_{1-x}Pd_x)Sb$[4−7] and $CeRh(Sb_{1-y}Sn_y)$.[8−11] One can also eliminate the 4f(Ce)−d(T) hybridization by substitution of the transition-metal component by another main group element, for example, in CeMgGa.[3]

Besides the chemical effects (substitution), also the parameter pressure plays an important role for a change of the physical properties. To give an example, electrical resistivity measurements on CePdSn with a standard DC four-probe technique in a cubic-anvil device up to 80 kbar[12] reveal disappearance of the magnetic transition above 60 kbar and transformation to a nonmagnetic Kondo lattice. Hydrostatic pressure experiments with high-resolution angle-

* Authors to whom correspondence should be addressed. E-mail: chevalie@icmcb-bordeaux.cnrs.fr (B.C.); pottgen@uni-muenster.de (R.P.).
† Université Bordeaux.
‡ Universität Münster.
§ Technische Universität Wien.

(1) Fujita, T.; Suzuki, T.; Nishigori, S.; Takabatake, T.; Fujii, H.; Sakurai, J. *J. Magn. Magn. Mater.* **1992**, *108*, 35.
(2) Szytuła, A.; Leciejewicz, J. *Handbook of Crystal Structures and Magnetic Properties of Rare Earth Intermetallics*; CRC Press: Boca Raton, FL, 1994.
(3) Kraft, R.; Pöttgen, R.; Kaczorowski, D. *Chem. Mater.* **2003**, *15*, 2998.
(4) Adroja, D. T.; Rainford, B. D. *J. Magn. Magn. Mater.* **1994**, *135*, 333.
(5) Menon, L.; Kayzel, F. E.; de Visser, A.; Malik, S. K. *Phys. Rev. B* **1998**, *58*, 85.
(6) Menon, L.; Malik, S. K. *Solid State Commun.* **1997**, *101*, 779.
(7) Menon, L.; Malik, S. K. *Phys. Rev. B* **1997**, *55*, 14100.
(8) Ślebarski, A.; Zawada, T.; Spałek, J.; Jezierski, A. *Phys. Rev. B* **2004**, *70*, 235112.
(9) Spałek, J.; Ślebarski, A.; Goraus, J.; Spałek, L.; Tomala, K.; Zarzycki, A.; Hackemer, A. *Phys. Rev. B* **2005**, *72*, 155112.
(10) Ślebarski, A.; Zawada, T.; Spałek, J. *Physica B* **2005**, *359−361*, 118.
(11) Ślebarski, A.; Spałek, J. *Phys. Rev. Lett.* **2005**, *95*, 046402.
(12) Iga, F.; Kasaya, M.; Suzuki, H.; Okayama, Y.; Takahashi, H.; Mori, N. *Physica B* **1993**, *186−188*, 419.

10.1021/cm0705338 CCC: $37.00
Published on Web 05/18/2007

dispersive X-ray powder diffraction using synchrotron radiation and the diamond anvil cell technique revealed a first-order phase transition at 8.7(7) GPa for CeAuGe.[13] The hexagonal NdPtSb-type arrangement transforms into an orthorhombic high-pressure modification with a TiNiSi-type crystal structure. CeNiSn, CePdSn, and CePtSn with orthorhombic TiNiSi type structure transform to the hexagonal structure type ZrNiAl through high-pressure−high-temperature treatment in a multianvil device.[14−16] These structural transitions are accompanied by changes in the magnetic properties.

Furthermore, modification of the physical properties occurs by hydrogenation. Several CeTX compounds have a hydrogen storage capacity up to two hydrogen atoms per formula unit. Hydrogenation leads to an increase of the unit cell volume and a decrease of the cerium valence. One observes a decrease of the hybridization between the 4f(Ce) orbitals and the conduction electrons induced by hydrogenation. In this scope, the hydrogenation can be considered as an application of negative pressure on the CeTX intermetallics.[17−24]

In the case of the CeTGa gallides, complete hydrogenation studies have been performed for T = Co, Ni, and Cu.[17,25,26] These ternary gallides form the hydrides $CeCoGaH_{3.0}$, $CeNiGaH_{1.1}$, and $CeCuGaH_{0.8}$ adopting AlB_2 related structures. With iridium as transition metal, $CeIrGaH_{1.7}$ has been reported.[27] Similar to the work reported by Hulliger,[28] about 8−10 wt % $CeIr_2$ as an impurity phase was observed. Susceptibility measurements revealed intermediate-valent behavior for CeRhGa[28] and CeIrGa[27] and paramagnetism for $CeIrGaH_{1.7}$.[27] In continuation of our recent studies on the hydrides of CeRhSn and CeIrSn,[29] we were interested in the corresponding gallium compounds. The synthesis, structures, and physical properties of Ce($Rh_{1-x}Ir_x$)Ga with $x = 0$, 0.54, and 1 and the corresponding hydrides Ce($Rh_{1-x}Ir_x$)$GaH_{1.8}$ are reported herein.

Experimental Section

Synthesis. Starting materials for the preparation of the ternary gallides Ce($Rh_{1-x}Ir_x$)Ga were sublimed cerium ingots (Johnson Matthey), rhodium and iridium powder (Degussa-Hüls), and gallium pieces (Merck), all with starting purities better than 99.9%. In a first step, pieces of the cerium ingot were arc-melted[30] to small buttons under an argon atmosphere of ca. 600 mbar. Argon was purified before using a titanium sponge (870 K), molecular sieves, and silica gel. The cerium buttons were then mixed with cold-pressed pellets (∅ 6 mm) of the respective noble metal and with pieces of gallium in the ideal 1:1:1 and 1:0.46:0.54:1 atomic ratios and were reacted in the same arc-melting crucible. The samples were turned over and remelted three times to ensure homogeneity. The total weight losses after the various melting procedures were always smaller than 0.5 wt %. The three ternary gallides were obtained as silvery pellets in amounts of ca. 1 g. They are stable in moist air over months in compact form and as powders. For CeIrGa, similar to the earlier reports,[27,28] we also observed a significant amount of the cubic Laves phase $CeIr_2$ as a side product after the first arc-melting step. This sample was reground, was cold-pressed to a pellet, and was arc-melted again to obtain an X-ray pure sample of CeIrGa.

Hydrogenation Reactions. The hydrogenation experiments were performed using an apparatus described previously.[31] About one-half of the arc-melted ingots of the three ternary gallides was heated under vacuum at 523 K for 12 h and then was exposed to 4 MPa of hydrogen gas at the same temperature. After 2 days, hydrogenation induced a decrepitation of the three ternary gallide samples. The amount of absorbed hydrogen was monitored volumetrically by measuring the pressure changes in a calibrated volume. This way, the hydrides Ce($Rh_{1-x}Ir_x$)$GaH_{1.8}$ ($x = 0$, 0.54, and 1) were obtained as black microcrystalline powders that are stable at ambient conditions.

X-ray Powder Data. The purity of the precursor ingots was checked by Guinier powder patterns, using $CuK_{\alpha 1}$ radiation and α-quartz ($a = 491.30$ and $c = 540.46$ pm) as an internal standard. The Guinier camera was equipped with an image plate system (Fujifilm, BAS-1800). The orthorhombic lattice parameters (Table 1) were derived from least-squares fits to the Guinier data. To ensure correct indexing of the patterns, the experimental ones were compared with calculated patterns[32] using the atomic positions obtained from the structure refinements. The powder lattice parameters compared well to those derived from the single crystals and to those obtained in previous studies.[27,28] The hydrogenated samples were characterized on a Philips 1050 powder diffractometer with CuK_α radiation. The refined hexagonal lattice parameters are listed in Table 1.

Energy-Dispersive X-ray (EDX) Analyses. The bulk samples of the precursors and the crystals investigated on the diffractometers were analyzed using a LEICA 420I scanning electron microscope with CeO_2, Rh, Ir, and GaP as standards. No impurity elements heavier than sodium (detection limit of the machine) were observed. The compositions determined by EDX (34 ± 3 at. % Ce:36 ± 3

(13) Brouskov, V.; Hanfland, M.; Pöttgen, R.; Schwarz, U. *Z. Kristallogr*. **2005**, *220*, 122.
(14) Riecken, J. F.; Heymann, G.; Soltner, T.; Hoffmann, R.-D.; Huppertz, H.; Johrendt, D.; Pöttgen, R. *Z. Naturforsch*. **2005**, *60b*, 821.
(15) Heymann, G.; Riecken, J. F.; Rayaprol, S.; Christian, S.; Pöttgen, R.; Huppertz, H. Z. *Anorg. Allg. Chem.* **2007**, *633*, 77.
(16) Heymann, G.; Riecken, J. F.; Hoffmann, R.-D.; Rodewald, U. Ch.; Rayaprol, S.; Huppertz, H.; Pöttgen, R. *Z. Kristallogr*. **2006**, *Suppl. 14*, 160.
(17) Chevalier, B.; Bobet, J.-L.; Pasturel, M.; Gaudin, E.; Etourneau, J. *J. Alloys Compd*. **2003**, *356−357*, 147.
(18) Chevalier, B.; Pasturel, M.; Bobet, J.-L.; Isnard, O. *Solid State Commun.* **2005**, *134*, 529.
(19) Chevalier, B.; Pasturel, M.; Bobet, J.-L.; Decourt, R.; Etourneau, J.; Isnard, O.; Sanchez Marcos, J.; Rodriguez Fernandez, J. *J. Alloys Compd*. **2004**, *383*, 4.
(20) Maehlen, J. P.; Stange, M.; Yartys, V. A.; Delaplane, R. G. *J. Alloys Compd*. **2005**, *404−406*, 112.
(21) Stange, M.; Paul-Boncour, V.; Latroche, M.; Percheron-Guégan, A.; Isnard, O.; Yartys, V. A. *J. Alloys Compd*. **2005**, *144*, 404−406.
(22) Bobet, J.-L.; Pasturel, M.; Chevalier, B. *Intermetallics* **2006**, *14*, 544.
(23) Chevalier, B.; Wattiaux, A.; Bobet, J.-L. *J. Phys.: Condens. Matter* **2006**, *18*, 1743.
(24) Chevalier, B.; Decourt, R.; Heying, B.; Schappacher, F. M.; Rodewald, U. Ch.; Hoffmann, R.-D.; Pöttgen, R.; Eger, R.; Simon, A. *Chem. Mater*. **2007**, *19*, 28.
(25) Chevalier, B.; Bobet, J.-L.; Gaudin, E.; Pasturel, M.; Etourneau, J. *J. Solid State Chem*. **2002**, *168*, 28.
(26) Chevalier, B.; Sanchez Marcos, J.; Rodriguez Fernandez, J.; Pasturel, M.; Weill, F. *Phys. Rev. B* **2005**, *71*, 214437.
(27) Raj, P.; Sathyamoorthy, A.; Shashikala, K.; Venkateswara Rao, R.; Malik, S. K. *Solid State Commun.* **2001**, *120*, 375.
(28) Hulliger, F. *J. Alloys Compd*. **1996**, *239*, 131.
(29) Chevalier, B.; Sebastian, C. P.; Pöttgen, R. *Solid State Sci.* **2006**, *8*, 1000.
(30) Pöttgen, R.; Gulden, Th.; Simon, A. *GIT Labor−Fachz.* **1999**, *43*, 133.
(31) Bobet, J.-L.; Pechev, S.; Chevalier, B.; Darriet, B. *J. Alloys Compd*. **1998**, *267*, 136.
(32) Yvon, K.; Jeitschko, W.; Parthé, E. *J. Appl. Crystallogr*. **1977**, *10*, 73.

Table 1. Lattice Parameters of Some Cerium Transition-Metal Gallides and Their Respective Hydrides

compound	structure type	*a*/pm	*b*/pm	*c*/pm	*V*/nm^3	reference
CeRhGa	TiNiSi	685.59(8)	437.73(4)	785.70(7)	0.2358	28
CeRhGa	TiNiSi	688.2(2)	439.6(1)	788.9(1)	0.2387	this work
$CeRhGaH_{1.8}$	ZrBeSi	437.3(1)	a	839.2(1)	0.1390	this work
$Ce(Rh_{0.46}Ir_{0.54})Ga$	TiNiSi	685.5(1)	436.0(1)	782.7(1)	0.2339	this work
$Ce(Rh_{0.46}Ir_{0.54})GaH_{1.8}$	ZrBeSi	440.1(1)	a	829.1(1)	0.1391	this work
CeIrGa	TiNiSi	702.6(3)	438.29(12)	782.11(13)	0.2408	28
CeIrGa	TiNiSi	689.3(1)	436.3(1)	783.5(1)	0.2356	27
CeIrGa	TiNiSi	690.1(1)	436.6(1)	785.2(2)	0.2366	this work
$CeIrGaH_{1.7}$	ZrBeSi	441.2	a	822.9	0.1387	27
$CeIrGaH_{1.8}$	ZrBeSi	441.8(1)	a	823.3(1)	0.1392	this work

Table 2. Crystal Data and Structure Refinement for CeRhGa, $Ce(Rh_{0.46}Ir_{0.54})Ga$, and CeIrGa with TiNiSi Type Structure, *Pnma*, $Z = 4$

empirical formula	CeRhGa	$Ce(Rh_{0.46}Ir_{0.54})Ga$	CeIrGa
molar mass	312.75 g/mol	360.97 g/mol	402.04 g/mol
unit cell dimensions	Table 1	Table 1	Table 1
calculated density	8.70 g/cm^3	10.15 g/cm^3	11.29 g/cm^3
crystal size	$20 \times 40 \times 40$ μm^3	$10 \times 20 \times 40$ μm^3	$20 \times 80 \times 160$ μm^3
detector distance			60 mm
exposure time			5 min
ω range; increment			0−180°, 1.0°
integr. param. A, B, EMS			15.0, 4.5, 0.018
transm. ratio (max/min)	6.67	3.88	3.10
absorption coefficient	36.4 mm^{-1}	62.0 mm^{-1}	85.9 mm^{-1}
F(000)	536	600	664
θ range	3−35°	3−35°	3−35°
range in *hkl*	±11, ±7, ±12	±11, ±7, ±12	±11, ±6, ±12
total no. reflections	2113	3812	3266
independent reflections	563 ($R_{int} = 0.1277$)	563 ($R_{int} = 0.1006$)	562 ($R_{int} = 0.0998$)
reflections with $I > 2\sigma$(I)	471 ($R_\sigma = 0.1163$)	463 ($R_\sigma = 0.0419$)	383 ($R_\sigma = 0.0931$)
data/parameters	563/20	563/21	562/20
goodness-of-fit on F^2	1.051	1.025	0.853
final R indices [$I > 2\sigma$ (I)]	R1 = 0.0250	R1 = 0.0299	R1 = 0.0379
	*w*R2 = 0.0467	*w*R2 = 0.0641	*w*R2 = 0.0776
R indices (all data)	R1 = 0.0350	R1 = 0.0415	R1 = 0.0607
	*w*R2 = 0.0493	*w*R2 = 0.0685	*w*R2 = 0.0810
extinction coefficient	0.0008(2)	0.0009(3)	0.0049(6)
largest diff. peak and hole	2.23/−3.07 e/Å^3	3.15/−2.90 e/Å^3	4.58/−4.63 e/Å^3

at. % Rh:30 ± 3 at. % Ga for the CeRhGa, 33 ± 3 at. % Ce:14 ± 2 at. % Rh:16 ± 2 at. % Ir:37 ± 3 at. % Ga for the $Ce(Rh_{0.46}Ir_{0.54})Ga$, and 33 ± 3 at. % Ce:34 ± 3 at. % Ir:33 ± 3 at. % Ga for the CeIrGa crystal) are in good agreement with the ideal 1:1:1 and 1:0.46:0.54:1 composition. The standard uncertainties account for the measurements performed at different parts of the bulk samples and the crystal. For the $Ce(Rh_{0.46}Ir_{0.54})Ga$ sample, a homogeneous distribution of rhodium and iridium was evident from pictures taken in backscattering mode.

X-ray Single-Crystal Data. Small irregular shaped single crystals of the three ternary gallides were directly selected from the crushed arc-melted samples. The crystals were mounted on quartz fibers using beeswax, and their quality for intensity data collection was then tested on a Buerger camera (also equipped with an image plate system) by Laue photographs. A suitable single crystal of each ternary gallide was then mounted on the diffractometer. Data of the CeRhGa and $Ce(Rh_{0.46}Ir_{0.54})Ga$ crystals were collected at room temperature using a four-circle diffractometer (CAD4) with graphite-monochromatized MoK_α radiation and a scintillation counter with pulse height discrimination. The scans were taken in $\omega/2\theta$ mode, and empirical absorption corrections based on psi-scan data, accompanied by spherical absorption corrections, were applied to the data sets. The CeIrGa crystal was measured on a Stoe IPDS-II diffractometer with MoK_α radiation in oscillation mode. A numerical absorption correction was applied to this data set. All relevant crystallographic data and details for the data collections and evaluations are listed in Table 2.

Physical Property Measurements. For the transport measurements, the hydride samples were compacted at room temperature (ca. 80% compactness) to pellets of 6 mm diameter and 3 mm thickness. The latter was heated for 2 days at 523 K under a pressure of 4 MPa hydrogen. Thermoelectric power measurements were performed on the pellets by a dynamic method. The measurement technique and the cell used are described elsewhere.[33] Bars of 1.5 × 1.5 × 5 mm^3 were cut from the layer pellets for the electrical resistivity measurements in the temperature range 4.2 K to room temperature. A standard DC four-probe technique was used. The contact wires were glued with a silver paste and an intensity current of 10 mA was used. Magnetization measurements were performed on another part of the pellets using a Superconducting Quantum Interference Device (SQUID) magnetometer in the temperature range 1.8−300 K and in applied fields up to 5 T. Heat capacity measurements were realized on a plate obtained from the pellet by a relaxation method with a Quantum Design PPMS system and by using a two-tau model analysis.

Results and Discussion

Structure Refinements. The close structural relationship of the three ternary gallides with CeRhGe and CeIrGe[34] was already evident from the Guinier powder patterns. The atomic positions of CeRhGe[34] were then taken as starting values, and the three structures were refined using SHELXL−97 (full-matrix least squares on F^2)[35] with anisotropic atomic displacement parameters for all atoms. For CeRhGa and

(33) Dordor, P.; Marquestaut, E.; Villeneuve, G. *Rev. Phys. Appl*. **1980**, *15*, 1607.
(34) Gaudin, E.; Chevalier, B.; Heying, B.; Rodewald, U. Ch.; Pöttgen, R. *Chem. Mater*. **2005**, *17*, 2693.
(35) Sheldrick, G. M. *SHELXL-97, Program for Crystal Structure Refinement*; University of Göttingen: Göttingen, Germany, 1997.

Table 3. Atomic Coordinates and Isotropic Displacement Parameters (pm^2) of CeRhGa, Ce(Rh$_{0.46}$Ir$_{0.54}$)Ga, and CeIrGa[a]

atom	Wyck.	*x*	*y*	*z*	U_{eq}
		CeRhGa			
Ce	4*c*	−0.03547(6)	1/4	0.68558(5)	66(1)
Rh	4*c*	0.73787(8)	1/4	0.38986(6)	86(1)
Ga	4*c*	0.3557(1)	1/4	0.43285(9)	79(2)
		Ce(Rh$_{0.46}$Ir$_{0.54}$)Ga			
Ce	4*c*	−0.03124(9)	1/4	0.68769(7)	54(2)
M	4*c*	0.73549(8)	1/4	0.38981(6)	63(2)
Ga	4*c*	0.3515(2)	1/4	0.43228(14)	64(3)
		CeIrGa			
Ce	4*c*	−0.02691(17)	1/4	0.69034(11)	59(5)
Ir	4*c*	0.73338(11)	1/4	0.39185(8)	69(5)
Ga	4*c*	0.3568(4)	1/4	0.4308(2)	63(4)

[a] U_{eq} is defined as one-third of the trace of the orthogonalized U_{ij} tensor. M = 46.0(8) % Rh + 54.0(8) % Ir.

Table 4. Interatomic Distances (pm) Calculated with the Powder Lattice Parameters of CeRhGa, Ce(Rh$_{0.46}$Ir$_{0.54}$)Ga, and CeIrGa[a]

CeRhGa				Ce(Rh$_{0.46}$Ir$_{0.54}$)Ga				CeIrGa			
Ce	1	Rh	280.6	Ce	1	M	282.7	Ce	1	Ir	286.9
	2	Rh	306.1		2	M	303.6		2	Ir	304.7
	2	Rh	306.3		2	M	303.8		2	Ir	305.0
	1	Ga	310.2		1	Ga	308.1		1	Ga	310.0
	2	Ga	318.9		2	Ga	315.2		2	Ga	314.2
	2	Ga	325.0		2	Ga	323.3		2	Ga	324.7
	1	Ga	335.0		1	Ga	329.9		1	Ga	328.7
	2	Ce	358.8		2	Ce	356.4		2	Ce	357.6
	2	Ce	369.4		2	Ce	368.3		2	Ce	372.0
Rh	1	Ga	265.2	M	1	Ga	264.4	Ir	2	Ga	264.8
	1	Ga	267.2		1	Ga	265.3		1	Ga	265.2
	2	Ga	268.4		2	Ga	265.5		1	Ga	268.5
	1	Ce	280.6		1	Ce	282.7		1	Ce	286.9
	2	Ce	306.8		2	Ce	303.6		2	Ce	304.7
	2	Ce	306.3		2	Ce	303.8		2	Ce	305.0
Ga	1	Rh	265.2	Ga	1	M	264.4	Ga	2	Ir	264.8
	1	Rh	267.2		1	M	265.3		1	Ir	265.2
	2	Rh	268.4		2	M	265.5		1	Ir	268.5
	1	Ce	310.2		1	Ce	308.1		1	Ce	310.0
	2	Ga	314.6		2	Ga	315.2		2	Ce	314.2
	2	Ce	318.9		2	Ce	316.6		2	Ga	322.8
	2	Ce	325.0		2	Ce	323.3		2	Ce	324.7
	1	Ce	335.0		1	Ce	329.9		1	Ce	328.7

[a] Standard deviations are all equal or less than 0.3 pm. All distances within the first coordination spheres are listed. M = 46% Rh + 54% Ir.

CeIrGa, all sites were fully occupied within two standard uncertainties. The Rh/Ir mixed occupancy of the Ce(Rh$_{0.46}$Ir$_{0.54}$)Ga crystal was refined as a least-squares variable. Final difference electron-density synthesis did not reveal any significant residual peaks. The results of the structure refinements are summarized in Table 2. The atomic coordinates and the interatomic distances are listed in Tables 3 and 4. Further information on the structure refinements is available. [Details may be obtained from Fachinformationszentrum Karlsruhe, D-76344 Eggenstein-Leopoldshafen (Germany) by quoting the Registry No's. CSD−417741 (CeRhGa), CSD−417743 (CeRh$_{0.46}$Ir$_{0.54}$Ga), and CSD−417742 (CeIrGa).]

Crystal Chemistry. The TiNiSi[36] related structures of CeRhGa, Ce(Rh$_{0.46}$Ir$_{0.54}$)Ga, and CeIrGa were refined from single-crystal diffractometer data for the first time. Our data confirm the previous X-ray powder data,[27,28] but the atomic positions have been refined with higher precision. Exemplary,

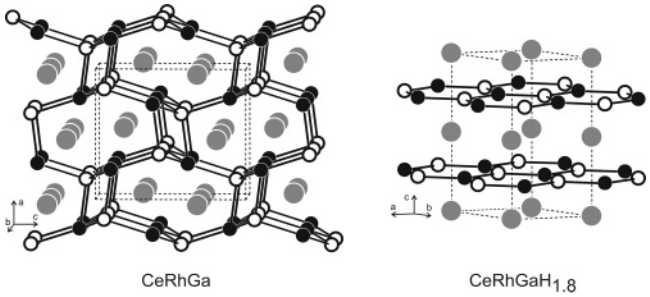

Figure 1. The crystal structures of CeRhGa and CeRhGaH$_{1.8}$. Cerium, rhodium, and gallium atoms are drawn as medium gray, black filled, and open circles, respectively. The three- and two-dimensional [RhGa] networks are emphasized. For details see text.

a view of the CeRhGa structure approximately along the *y*-axis is presented in Figure 1. The rhodium and gallium atoms build up a three-dimensional [RhGa] network with Rh−Ga distances ranging from 265 to 268 pm (Table 4), slightly longer than the sum of the covalent radii of 250 pm.[37] Within the network, each rhodium atom has a strongly distorted tetrahedral gallium coordination and vice versa. This situation is similar for the structures of Ce(Rh$_{0.46}$Ir$_{0.54}$)Ga and CeIrGa. Since the crystal chemistry of TiNiSi related intermetallics has been described in detail in several review articles,[38−42] here we focus only on the structural peculiarities of the ternary gallides with respect to CeRhGe and CeIrGe.[34]

The TiNiSi related compounds derive from the AlB_2 type by a strong puckering of the hexagonal networks, leading to interlayer Rh−Ga and Ir−Ga interactions in the compounds investigated (Figure 1). The degree of puckering strongly depends on the nature of the T and X component. Because of the puckering, one observes formation of T_2X_2 parallelograms between the hexagonal nets. Nuspl et al.[38] recently demonstrated that always the more electronegative element shows the position with the maximal distance (repulsion minimization) within the parallelogram. These parallelograms are shown together with the cerium near-neighbor coordinations in Figure 2. The tilting pattern of the Rh_3Ga_3 hexagons in CeRhGa compares well with the Ir_3Ge_3 hexagons in CeIrGe, while a completely different tilt is observed in CeRhGe. These tilts are directly related to the valence of the cerium atoms. In CeRhGa, Ce(Rh$_{0.46}$Ir$_{0.54}$)Ga, CeIrGa, and CeIrGe, where the cerium atoms exhibit an intermediate valence behavior, we observe very short Ce−Rh (281 pm in CeRhGa and 283 pm in Ce(Rh$_{0.46}$Ir$_{0.54}$)Ga) (Table 4) and Ce−Ir (287 pm in CeIrGa and 295 pm in CeIrGe) distances which are close to or even shorter than the sums of the covalent radii[37] (290 pm for Ce + Rh and 291 pm for Ce + Ir). Since the rhodium and iridium atoms are the most electronegative component in these phases, the close distance to the intermediate valent cerium atoms allows for an optimal charge compensation. The strong tilt of the hexagons is directly evident from the atomic positions. CeRhGa which

(36) Shoemaker, C. B.; Shoemaker, D. P. *Acta Crystallogr*. **1965**, *18*, 900.
(37) Emsley, J. *The Elements*; Clarendon Press: Oxford, U.K., 1989.
(38) Nuspl, G.; Polborn, K.; Evers, J.; Landrum, G. A.; Hoffmann, R. *Inorg. Chem*. **1996**, *35*, 6922.
(39) Landrum, G. A.; Hoffmann, R.; Evers, J.; Boysen, H. *Inorg. Chem*. **1998**, *37*, 5754.
(40) Hoffmann, R.-D.; Pöttgen, R. *Z. Kristallogr*. **2001**, *216*, 127.
(41) Bojin, M. D.; Hoffmann, R. *Helv. Chim. Acta* **2003**, *86*, 1653.
(42) Bojin, M. D.; Hoffmann, R. *Helv. Chim. Acta* **2003**, *86*, 1683.

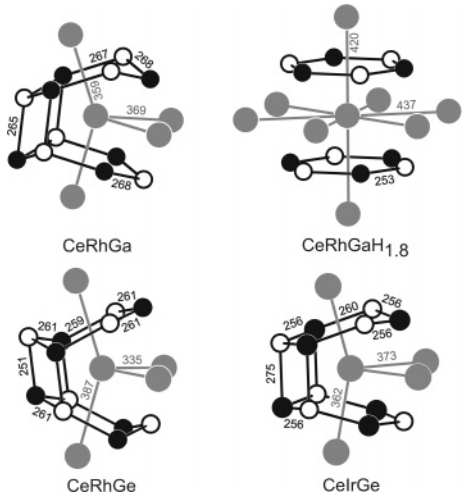

Figure 2. Coordination of the cerium atoms in the structures of CeRhGa, $CeRhGaH_{1.8}$, CeRhGe, and CeIrGe. The transition metal and X atoms are drawn as filled and open circles, respectively. The interatomic distances are expressed in pm.

has the shortest Ce−Rh distance has the largest x_{Ce} and the smallest z_{Ce} parameter (Table 3) among the four compounds discussed. This extreme situation in CeRhGa is also evident from the very large Rh−Rh distance of 431 pm which is even much larger than in CeIrGe (391 pm).[34] According to the argumentation by Nuspl et al.,[38] this is clear evidence for accumulation of electron density at the rhodium and iridium atoms in CeRhGa and CeIrGe, respectively.

In the 9.3 K antiferromagnet CeRhGe[34] with purely trivalent cerium, the situation is different. The Rh_3Ge_3 hexagons show the inverse tilt, and we observe the longer Ce−Rh distance of 302 pm (Figure 2). Since recent electronic structure calculations on CeRhGe[43] revealed extremely strong Ce−Rh interactions, we can assume even stronger interactions for CeRhGa discussed herein. Each cerium atom in the three ternary gallides has four closest cerium neighbors at Ce−Ce distances in the range from 356 to 372 pm, close to the Ce−Ce distance in face-centered cubic (fcc) cerium (365 pm)[44] and above the Hill limit for 4f electron localization.[45]

Now, we turn to the hydride phases $CeRhGaH_{1.8}$, $Ce(Rh_{0.46}Ir_{0.54})GaH_{1.8}$, and $CeIrGaH_{1.8}$. Hydrogenation of the ternary gallides leads to a significant increase of the unit cell volume per formula unit by 18% and a change in crystal structure. The X-ray powder pattern readily revealed hexagonal unit cells for the hydride phases. The intensity distribution was compatible with a ZrBeSi type[46] arrangement for the metal atoms with planar Rh_3Ga_3 hexagons. Since the resolution of the powder patterns is limited, a small degree of puckering cannot be excluded. The $CeRhGaH_{1.8}$ structure is presented as an example in Figure 1.

Since for the ZrBeSi type (space group $P6_3/mmc$) only special positions are occupied (Ce in the 2*a* site (000), Rh or Ir in the 2*c* site ($^1/_3{}^2/_3{}^1/_4$), and Ga in the 2*d* site ($^1/_3{}^2/_3{}^3/_4$),

Table 5. Interatomic Distances (pm), Calculated with the Powder Lattice Parameters of $CeRhGaH_{1.8}$, $Ce(Rh_{0.46}Ir_{0.54})GaH_{1.8}$, and $CeIrGaH_{1.8}$[a]

$CeRhGaH_{1.8}$				$Ce(Rh_{0.46}Ir_{0.54})GaH_{1.8}$				$CeIrGaH_{1.8}$			
Ce	6	Rh	328.3	Ce	12	M	327.9	Ce	6	Ir	327.8
	6	Ga	328.3		2	Ce	414.6		6	Ga	327.8
	2	Ce	419.6		6	Ce	440.1		2	Ce	411.6
	6	Ce	437.3						6	Ce	441.8
Rh	3	Ga	252.5	M	3	M	254.1	Ir	3	Ga	255.1
	6	Ce	328.3		6	Ce	327.9		6	Ce	327.8
Ga	3	Rh	252.5					Ga	3	Ir	255.1
	6	Ce	328.3						6	Ce	327.8

[a] Standard deviations are all equal to or less than 0.1 pm. All metal−metal distances within the first coordination spheres are listed. M = 46% Rh + 54% Ir.

the interatomic distances for the metal sites can directly be calculated from the lattice parameters. The corresponding coordination polyhedron of the cerium atoms and the relevant interatomic distances are given in Figure 2. Hydrogenation leads to drastic changes in the bonding pattern. The puckered hexagons of CeRhGa become planar and the pseudohexagonal axis significantly enlarges. The Rh−Ga networks are (almost) planar with shorter Rh−Ga distances of 253 pm (Table 5), close to the sum of the covalent radii. We thus observe an increase of Rh−Ga bonding. On the other hand, the Ce−Ce distances become much longer. The ZrBeSi type leaves two reasonable tetrahedral [Ce_3Rh or Ce_3Ir] voids per formula unit, and according to the volumetric measurements, these are almost filled in the three ternary gallides. It was recently reported using neutron powder diffraction that similar [La_3Ni] tetrahedra were completely occupied by deuterium in $LaNiSnH_2$ adopting also the hexagonal ZrBeSi-type.[47]

Finally, we need to comment on the course of the lattice parameters in the series $CeRhGaH_{1.8}$, $Ce(Rh_{0.46}Ir_{0.54})GaH_{1.8}$, and $CeIrGaH_{1.8}$. With increasing iridium content, the *a* lattice parameter increases while *c* decreases; consequently, the *c*/*a* ratio decreases continuously from 1.92 ($CeRhGaH_{1.8}$) to 1.86 ($CeIrGaH_{1.8}$) (Table 1). As usually observed in isotypic series of rhodium and iridium compounds, for example, CeRhGe and CeIrGe,[34] or $SmRhIn_2$[48] and $SmIrIn_2$,[49] the iridium compounds show the slightly larger Ir−X distances. To keep similar Ce−T and Ce−Ga distances in the hydrides $CeRhGaH_{1.8}$, $Ce(Rh_{0.46}Ir_{0.54})GaH_{1.8}$, and $CeIrGaH_{1.8}$, the *c* parameter needs to contract (Table 5). This behavior is similar to the germanide hydrides $CeRhGeH_{1.8}$ and $CeIrGeH_{1.8}$.[50] Also in the hydrides $Ce(Rh_{1-x}Ir_x)GaH_{1.8}$, the unit cell volume *V* (Table 1) increases weakly with the iridium content in agreement with the increase of the covalent radii in the sequence Rh → Ir.

The structural transition orthorhombic TiNiSi type → hexagonal ZrBeSi type observed during the hydrogenation of the ternary gallides $Ce(Rh_{1-x}Ir_x)Ga$ is similar to that previously observed by H-insertion into CeNiGe,[19,51] Ce-

(43) Matar, S.; Gaudin, E.; Chevalier, B.; Pöttgen, R. *Solid State Sci.*, **2007**, *9*, 274.
(44) Donohue, J. *The Structure of the Elements*; Wiley: New York, 1974.
(45) Hill, H. H. In *Plutonium and Other Actinides*; Mines, W. N., Ed.; Nuclear Materials Series, AIME; 1970; Vol. 17, p 2.
(46) Nielsen, J. W.; Baenziger, N. C. *Acta Crystallogr*. **1954**, *7*, 132.
(47) Yartys, V. A.; Olavesen, T.; Hauback, B. C.; Fjellvag, H.; Brinks, H. W. *J. Alloys Compd*. **2002**, *330*−*332*, 141.
(48) Zaremba, V. I.; Dubenskiy, V. P.; Pöttgen, R. *Z. Naturforsch*. **2002**, *57b*, 798.
(49) Zaremba, V. I.; Rodewald, U. Ch.; Pöttgen, R. *Z. Anorg. Allg. Chem*. **2005**, *631*, 1065.
(50) Chevalier, B.; Pöttgen, R. Unpublished results.

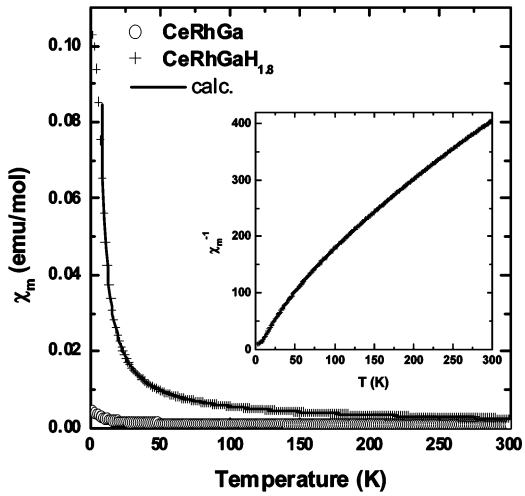

Figure 3. Temperature dependence of the magnetic susceptibility, measured with an applied field $\mu_0 H = 4$ T, of CeRhGa and its hydride. Solid line shows the fit to calculated χ_m, using the crystal field effect and the molecular field (see text). The inset presents the reciprocal magnetic susceptibility of $CeRhGaH_{1.8}$ versus temperature.

NiGa,[19,25,26] CeNiSn,[19,52] CeRhGe, and CeIrGe.[50] This transition induces an increase of both the unit cell volume and the interatomic distances existing between the Ce atom and its nearest neighbors as Ni, Rh, Ir, Ge, Ga, or Sn. All these steric considerations suggest a strong modification of the strength of 4f(Ce)-ligand interactions responsible for the electronic state of cerium in these intermetallics. For instance, the hydrogenation of CeNiGe or CeNiSn reveals a decrease of the Kondo temperature for the former[51] or the occurrence of a ferromagnetic state for the ternary stannide.[52]

Magnetic Properties. Figure 3 presents the temperature dependence of the magnetic susceptibility χ_m of CeRhGa and its hydride. An appreciable increase in the χ_m value of the hydride is observed relative to that of CeRhGa.

Above 75 K, χ_m of CeRhGa is practically independent of the temperature characterizing an intermediate valence state of the cerium having a high Kondo temperature. The increase of χ_m at low temperatures is mainly attributed to the presence of trace amounts of stable moment Ce^{3+} ions from magnetic impurities such as Ce_2O_3. The $\chi_m = f(T)$ curve can be fitted according to $\chi_m = \chi_0 + nC/T$, where χ_0 is the temperature-independent part of the susceptibility and n is the proportion of stable Ce^{3+} moments ($C = 0.807$ emu K/mol) in the ternary gallide. This procedure gives $\chi_0 = 9.62\ 10^{-4}$ emu/mol and $n = 18 \times 10^{-3}$. The observed χ_0 value can be discussed in terms of a characteristic temperature T_K related to Kondo-type fluctuations.[53] In this scheme, T_K is defined as $T_K = C/2\chi_0$ and can be estimated at 420 K. This behavior is comparable to that observed previously for CeIrGa.[27]

The curve $\chi_m = f(T)$ of the hydride $CeRhGaH_{1.8}$ does not follow a simple Curie−Weiss law (see inset of Figure 3). Similar behavior was observed previously for $CeNiSnH_{1.8}$ which adopts also the hexagonal ZrBeSi type.[52] Deviations from this law are, most likely, related to crystal field effects (CEF). For the hexagonal symmetry, the Ce $^2F_{5/2}$ state is split into three doublets: $\Gamma_7 = |\pm 1/2\rangle$, $\Gamma_8 = |\pm 5/2\rangle$, and $\Gamma_9 = |\pm 3/2\rangle$. In the paramagnetic range, the temperature dependence of the magnetic susceptibility $\chi_m = f(T)$ can be expressed in terms of hexagonal crystal field splitting of the $J = 5/2$ total angular momentum and of molecular field effects, that is,[54,55]

$$\chi_m = \chi_0 + \chi_{CF} - \lambda$$

where χ_0 is the temperature-independent part of the susceptibility, χ_{CF} is the susceptibility due to the crystal field effects, and λ is the molecular field parameter. For analyses based on data from polycrystalline sample, χ_m is given by

$$\chi_m = \frac{1}{3}\chi_{||} + \frac{2}{3}\chi_{\perp}$$

where $\chi_{||}$ and $\chi_{\perp}$ are the components of the uniform susceptibility parallel and perpendicular to the c-axis, respectively. Using the calculation described previously,[52] the most satisfying fit to the data of $CeRhGaH_{1.8}$ (solid line, Figure 3) is then obtained for $\chi_0 = 0.3 \times 10^{-3}$ emu/mol, $\lambda_{\perp} = -165$ mol/emu, and $\lambda_{||} = 9.5$ mol/emu. Moreover, this calculation indicates that (1) the doublet $\Gamma_9 = |\pm 3/2\rangle$ is the ground state and that (2) it is separated by 37 and 64 K from the first $\Gamma_8 = |\pm 5/2\rangle$ and the second $\Gamma_7 = |\pm 1/2\rangle$ excited levels, respectively. The ground-state doublet is close to both excited states. Since data from polycrystalline material were used, the derived crystal field scheme is only tentative and has to be confirmed by single-crystal data by inelastic neutron scattering investigation and by specific heat measurements at higher temperatures. A same Γ_9 ground state was reported in the case of the isostructural hydride $CeNiSnH_{1.8}$.[52]

Similar analysis performed on the two other hydrides gives $\chi_0 = 0.45 \times 10^{-3}$ emu/mol, $\lambda_{\perp} = -135$ mol/emu, and $\lambda_{||} = -3$ mol/emu for $Ce(Rh_{0.46}Ir_{0.54})GaH_{1.8}$ and $\chi_0 = 0.5 \times 10^{-3}$ emu/mol, $\lambda_{\perp} = -193$ mol/emu, and $\lambda_{||} = -8$ mol/emu for $CeIrGaH_{1.8}$. The ground state is always the Γ_9 doublet, but we observe Γ_7 and Γ_8 as the first and the second excited levels; the energy splittings are, respectively, 14 and 20 K for $Ce(Rh_{0.46}Ir_{0.54})GaH_{1.8}$ and 80 and 97 K for $CeIrGaH_{1.8}$. The different splitting schemes observed for $CeRhGaH_{1.8}$ on the one hand and for $Ce(Rh_{0.46}Ir_{0.54})GaH_{1.8}$ and $CeIrGaH_{1.8}$ on the other hand could be explained by a decrease of the c/a ratio (Table 1) from 1.92 to 1.86 with increasing the iridium content in the hydride. All these results agree with the presence of trivalent cerium in the hydrides $Ce(Rh_{1-x}Ir_x)GaH_{1.8}$. In other words, the hydrogenation of the $Ce(Rh_{1-x}Ir_x)Ga$ system induces a cerium valence transition from an intermediate valent to a trivalent state.

At low temperature, the thermal dependence of the magnetization M of $CeRhGaH_{1.8}$ divided by the applied field shows a kink at $T_N = 4.8(2)$ K (temperature where the derivative curve $d(M/\mu_0 H)/dT = f(T)$ exhibits a maximum) (Figure 4). This behavior suggests that this hydride orders antiferromagnetically. The increase of M below T_N indicates that this ordering is strongly influenced by the applied field.

(51) Chevalier, B.; Pasturel, M.; Bobet, J.-L.; Weill, F.; Decourt, R.; Etourneau, J. *J. Solid State Chem.* **2004**, *177*, 752.
(52) Chevalier, B.; Bobet, J.-L.; Pasturel, M.; Bauer, E.; Weill, F.; Decourt, R.; Etourneau, J. *Chem. Mater.* **2003**, *15*, 2181.
(53) Lawrence, J. M. *Phys. Rev. B* **1979**, *20*, 3770.
(54) Kitazawa, H.; Schank, C.; Thies, S.; Seidel, B.; Geibel, C.; Steglich, F. *J. Phys. Soc. Jpn.* **1992**, *61*, 1461.
(55) Schröder, A.; Van den Berg, R.; Löhneysen, H. v.; Paul, W.; Lueken, H. *Solid State Commun.* **1988**, *65*, 99.

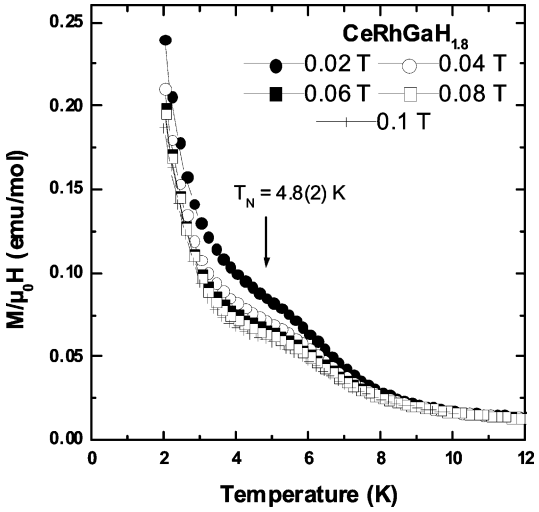

Figure 4. Temperature dependence of the magnetization of $CeRhGaH_{1.8}$ divided by different applied magnetic fields.

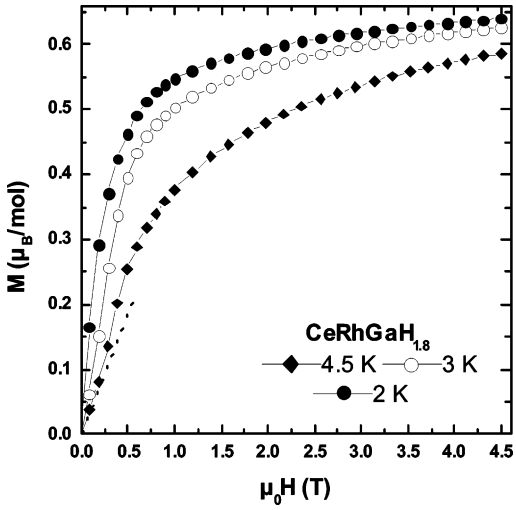

Figure 5. Field dependence of the magnetization of $CeRhGaH_{1.8}$ measured at $T = 2$, 3, and 4.5 K. The dotted line emphasizes a metamagnetic behavior above 0.2 T at 4.5 K.

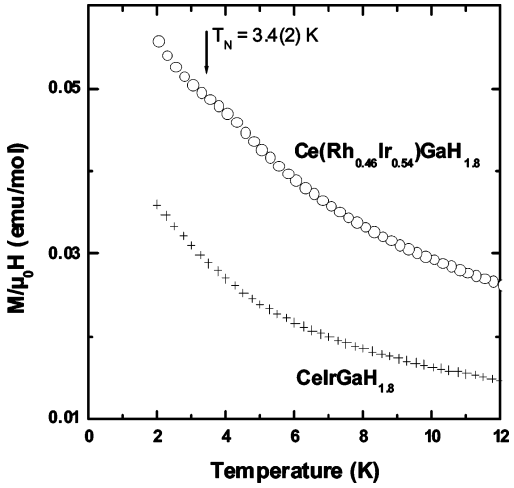

Figure 6. Temperature dependence of the magnetization of $Ce(Rh_{0.46}Ir_{0.54})GaH_{1.8}$ and $CeIrGaH_{1.8}$ divided by applied magnetic field (0.1 T).

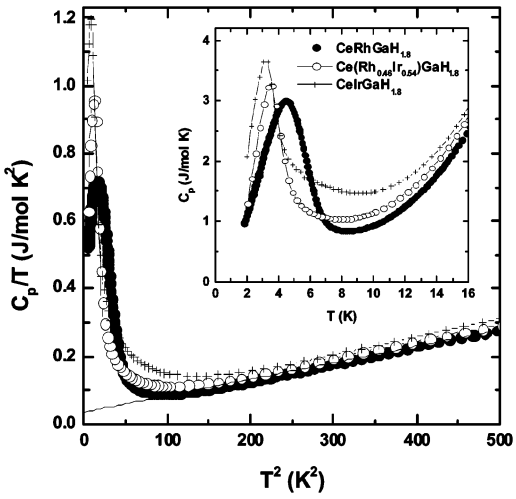

Figure 7. Plots C_p/T versus T^2 for the hydrides $Ce(Rh_{1-x}Ir_x)GaH_{1.8}$. The solid line shows the fitting of $C_p/T = \gamma + \beta T^2$ for $CeRhGaH_{1.8}$ (see text). The inset presents the temperature dependence of the specific heat C_p in the three hydrides.

This is further corroborated by the field-dependent behavior of M below T_N (Figure 5) with, for instance, a distinct metamagnetic-like anomaly above 0.2 T at 4.5 K. In high magnetic fields, M shows a tendency to saturation reaching at 4.5 T a value of 0.64(2) μ_B/mol. This Ce-magnetic moment is comparable to that previously observed in the hydride $CeNiSnH_{1.8}$[52] and corroborates the lifting of the 6-fold degenerate ground state of the Ce ions by CEF effects. Furthermore, the Kondo effect gives rise to an additional reduction of the ordered moments (see also below).

The low-temperature magnetization data for $Ce(Rh_{0.46}Ir_{0.54})GaH_{1.8}$ and $CeIrGaH_{1.8}$ reveal (Figure 6) (1) the occurrence of a very small shoulder at $T_N = 3.4(2)$ K for the former and (2) down to 1.8 K any anomaly that suggests an onset of antiferromagnetic ordering. In the $Ce(Rh_{1-x}Ir_x)GaH_{1.8}$ series, the Néel temperature decreases with increasing iridium content.

Thermal Properties. The temperature dependence of the specific heat C_p of the three hydrides shows a well-defined peak (see inset of Figure 7). The curves $C_p = f(T)$ for $CeRhGaH_{1.8}$ and $Ce(Rh_{0.46}Ir_{0.54})GaH_{1.8}$ exhibit a maximum at 4.5(2) K and 3.5(2) K, respectively. These temperatures are in agreement with those determined by magnetization measurements (Figures 4 and 6) confirming the occurrence of antiferromagnetic ordering for these hydrides. Surprisingly, a similar peak appears at 3.2(2) K in the curve $C_p = f(T)$ concerning $CeIrGaH_{1.8}$ suggesting a magnetic transition not detected by magnetization measurements, see Figure 6 and ref 27.

Valuable information can be obtained from the entropy associated with the magnetic ordering of these hydrides, which is estimated from the magnetic contribution to the specific heat in the low-temperature range as $C_{pmag} = C_p - (\gamma T + \beta T^3)$. For instance, between 10 and 22 K, the fitting of $C_p/T = \gamma + \beta T^2$ for $CeRhGaH_{1.8}$ (Figure 7) yields an electronic coefficient $\gamma = 35$ mJ/Ce-mol K^2 and a phonon constant $\beta = 4.86\ 10^{-4}$ J/Ce-mol K^4. At $T_N = 4.5(2)$ K, the magnetic entropy reaches 1.82 J/Ce-mol K = 0.32 Rln2 which is smaller than Rln2 = 5.76 J/Ce-mol K, the value of magnetic entropy expected for a doublet ground state of Ce^{3+}. Thus, there is a considerable reduction of magnetic entropy because of the Kondo effect. Moreover, the same fitting applied to the hydrides $Ce(Rh_{0.46}Ir_{0.54})GaH_{1.8}$ and $CeIrGaH_{1.8}$

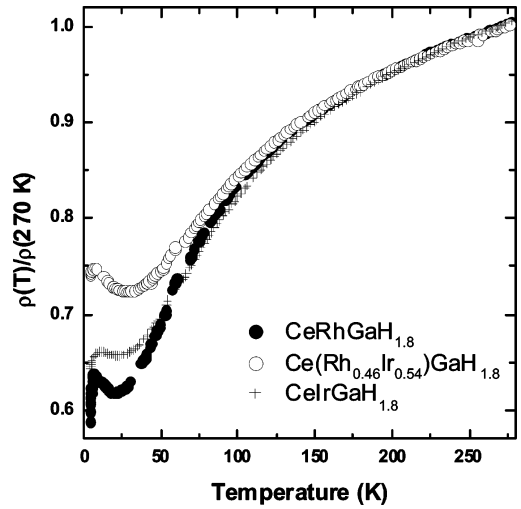

Figure 8. Temperature dependence of the normalized electrical resistivity for the hydrides Ce(Rh$_{1-x}$Ir$_x$)GaH$_{1.8}$.

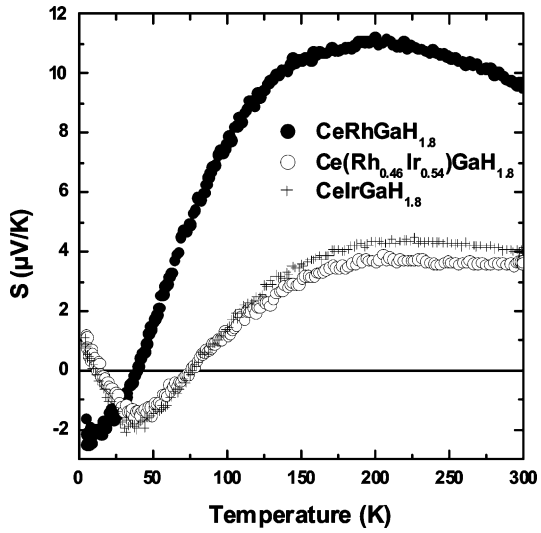

Figure 9. Temperature dependence of the thermoelectric power for the hydrides Ce(Rh$_{1-x}$Ir$_x$)GaH$_{1.8}$.

gives similar magnetic entropy (1.74 and 1.93 J/Ce-mol K, respectively) but an increase of the γ-value (55 mJ/Ce-mol K^2 for the two hydrides) with increasing iridium content. This suggests a small increase of the hybridization between the 4f(Ce) orbitals and the conduction electrons in the sequence CeRhGaH$_{1.8}$ → CeIrGaH$_{1.8}$

Electrical Properties. Figure 8 depicts the temperature-dependent normalized electrical resistivity, measured above 4.2 K, for the three hydrides Ce(Rh$_{1-x}$Ir$_x$)GaH$_{1.8}$. (Because of the presence of porosities and microcracks resulting from the low temperature (523 K) used during the annealing treatment performed on these samples, the absolute value of $\rho(T)$ could not be determined accurately; for this reason, the normalized resistivity is reported). The ratio ρ(270 K)/ρ(4.2 K) = 1.72, which is similar for the hydrides with x = 0 and 1, is smaller (1.35) for x = 0.54. This results from the atomic disorder induced by the presence of rhodium and iridium atoms on the same crystallographic site (Table 5).

For both hydrides, $\rho(T)/\rho(270\ \mathrm{K}) = \mathrm{f}(T)$ deviates from a normal metallic behavior, displaying features usually associated to the Kondo effect as observed, for example, for CeAl$_2$.[56] For instance, $\rho(T)$ of CeRhGaH$_{1.8}$ shows (1) a downward curvature around 120−200 K associated to the influence of the Kondo effect on the excited doublet of cerium and (2) a minimum at 20 K and a maximum near 5 K; between these two temperatures, a behavior according to $-A \log T$ (A = constant) is observed, in agreement with the Kondo effect from the crystal field ground state (incoherent Kondo scattering). Finally, the decrease of $\rho(T)/\rho(270\ \mathrm{K})$ below 5 K is associated to the loss of spin disorder scattering of the conduction electrons owing to the appearance of an antiferromagnetic transition (for this hydride, T_N = 4.8(2) K as determined by magnetization measurements).

$\rho(T)/\rho(270\ \mathrm{K}) = \mathrm{f}(T)$ for the other hydrides Ce(Rh$_{0.46}$Ir$_{0.54}$)GaH$_{1.8}$ and CeIrGaH$_{1.8}$ behave similarly; the increase of the resistivity followed by a decrease observed for $T <$ 20−24 K suggests for these hydrides a Kondo-lattice behavior exhibiting a magnetic transition. The temperature where these curves exhibit a minimum is practically constant (20−24 K) for both hydrides showing a same influence of the Kondo effect.

Thermoelectric Properties. Figure 9 shows the temperature dependence of the thermoelectric power S of the hydrides Ce(Rh$_{1-x}$Ir$_x$)GaH$_{1.8}$. $S = \mathrm{f}(T)$ of CeRhGaH$_{1.8}$ is characterized by the existence of two extremes: a positive maximum of about 11 μV/K around 200 K and a negative one at −2 μV/K near 12 K. Such behavior is commonly observed in Ce-based Kondo-lattice systems having a low Kondo temperature (nearly trivalent) as CeAl$_2$.[57] S can be qualitatively understood in terms of the Coqblin-Schrieffer model (CSM) which describes the dynamics of conduction electrons because of the exchange and potential scattering on incoherent 4f(Ce) states.[58,59] This model uses the crystalline electric field (CEF) (Δ as energy separation between ground and excited levels) and the number of 4f(Ce) electrons ($n_f \leq 1$ for cerium). S of CeRhGaH$_{1.8}$ follows within the CSM model for moderate CEF splitting and $n_f \leq 1$ (nearly trivalent cerium having a low Kondo temperature). The temperature ≅ 200 K of the positive maximum is comparable to that where the curve $\rho(T)/\rho(270\ \mathrm{K}) = \mathrm{f}(T)$ (Figure 8) exhibits a downward curvature. These two measurements are in agreement for the qualitative determination of the CEF splitting in the hydride CeRhGaH$_{1.8}$. Finally, S changes sign around 38 K. This last behavior was explained recently using CEF splittings and the coupling constant Γ which measures the coupling strength between the 4f(Ce) orbitals and the conduction band.[60,61] This zero crossing characterizes the Kondo systems having small Kondo temperature.

The curves $S = \mathrm{f}(T)$ of the two other hydrides (1) present a positive maximum at 200−220 K, a temperature comparable to that determined for CeRhGaH$_{1.8}$ suggesting a similar CEF splitting as shown by magnetization measurements, and

(56) Cornut, B.; Coqblin, B. *Phys. Rev. B* **1972**, *5*, 4541.
(57) Garde, C. S.; Ray, J. *Phys. Rev. B* **1995**, *51*, 2960.
(58) Zlatic, V.; Milat, I.; Coqblin, B.; Czycholl, G. *Physica B* **2002**, *171*, 312−313.
(59) Zlatic, V.; Horvatic, B.; Milat, I.; Coqblin, B.; Czycholl, G.; Grenzebach, C. *Phys. Rev. B* **2003**, *68*, 104432.
(60) Zlatic, V.; Monnier, R. *Phys. Rev. B* **2005**, *71*, 165109.
(61)) Wilhelm, H.; Jaccard, D.; Zlatic, V.; Monnier, R.; Delley, B.; Coqblin, B. *J. Phys.: Condens. Matter* **2005**, *17*, S823.

(2) show a higher temperature (78 K) where *S* changes sign. This result suggest that the coupling constant Γ is modified for these two hydrides containing iridium.

Conclusion

Hydrogen sorption in the intermediate-valent orthorhombic TiNiSi type gallides $Ce(Rh_{1-x}Ir_x)Ga$ with $x = 0$, 0.54, and 1 leads to the hydrides $Ce(Rh_{1-x}Ir_x)GaH_{1.8}$ with hexagonal ZrBeSi type structure. The hydrogenation leads to a switch in the magnetic properties from intermediate valence to stable trivalent cerium in the hydrides, accompanied by antiferromagnetic ordering at low temperatures. The three hydrides have the doublet $\Gamma_9 = |\pm^3/_2$ as ground state. Temperature-dependent resistivity data and measurements of the thermoelectric power revealed metallic behavior for the hydrides and are indicative for moderate Kondo type interactions.

Acknowledgment. The authors would like to thank R. Decourt for his assistance during the electrical resistivity and thermoelectric power measurements. This work was financially supported by the Deutsche Forschungsgemeinschaft. B.C. and R.P. are indebted to EGIDE and DAAD for research grants within the Procope programs (11457RD and D/0502176). Finally, B.C. thanks the European Science Foundation (ECOM-COST action P16) for financial support. C.P.S. is indebted to the NRW Graduate School of Chemistry for a PhD stipend, and E.B. acknowledges support by the Austrian FWF, P19165.

Supporting Information Available: Crystallographic information (CIF). This material is available free of charge via the Internet at http://pubs.acs.org.

CM0705338